

Effect of controlled doping on electrical properties and permittivity of PTSA doped polyanilines and their EMI shielding performance

Parveen Saini^{1*}, Manju Arora¹, S K Arya² & Jai S Tawale¹

¹CSIR-National Physical Laboratory, Dr K S Krishnan Road, New Delhi 110 012, India

²School of Physics and Materials Science, Thapar University, Patiala 147 004, India

*E-mail: pksaini@nplindia.org

Received 16 September 2013; revised 8 January 2014; accepted 30 January 2014

Emeraldine base (EB) has been protonated with different concentration of *para*-toluene sulfonic acid (PTSA) to form doped polyanilines (PANIs). These samples have been characterized by various techniques and a detailed correlation between dopant concentration and structural, thermal, electrical and electromagnetic properties has been established. The FTIR/UV-Visible and EPR spectra confirm the formation of polarons as proto-generated charge carriers whose concentration follows the dopant concentration trend. It was also observed that increase in doping level leads to systematic improvement of electrical conductivity (1.2×10^{-9} to 5.3 S/cm) as well as complex permittivity ($\epsilon' \sim 5.5$ & $\epsilon'' \sim 0.6$ to $\epsilon' \sim 22.3$ & $\epsilon'' \sim 24.6$) with parallel improvement of electromagnetic (EM) radiation blocking capacity from -3.8 dB (for EB) to -23.9 dB (for 1.0 M PTSA doped sample). Further, the attenuation was found to be critically dependent on dopant concentration, complex permittivity and electrical conductivity revealing that both polarization as well as conduction is important for achieving high attenuation. It was also observed that reflection is main phenomenon at low doping level whereas absorption becomes increasingly important at higher doping levels and extends dominant contribution towards total attenuation.

Keywords: Electromagnetic interference shielding, Complex permittivity, Polyaniline, Electrical conductivity, EPR spectroscopy, TGA

1 Introduction

The rapid growth of electronics and its prevalence in the areas of communication, surveillance, medical science, aerospace, defense and even daily life has produced a novel kind of pollution known as electromagnetic (EM) interference¹⁻³ (EMI). The interfering EM radiations from variety of sources and electronic circuitry may disturb or even completely disrupt the performance of electronic instruments/appliances^{4,5}. The recent research has categorized prolonged exposure to EM radiation as carcinogen whereas irregular dosages and short exposures are known to cause troubles like amnesia, insomnia, depressions, nausea, giddiness, brain/heart strokes, miscarriages or even leukemia, brain/breast tumors under extreme conditions^{1,2,6,7}. Therefore, suitable counter-measures are necessary to ensure EMI free performance of the electronic gadgets and to protect the societal health. Generally, conducting compositions based on metals, graphite, and carbon nanotubes (CNTs) are used for EMI shielding due to their high conductivity and good dielectric properties¹⁻⁵. However, metals have disadvantages of high density, corrosion susceptibility and difficult processing whereas graphite needs high percolation thresholds⁶⁻⁹.

Likewise, CNT are economically non-viable, difficult to produce at bulk scale and often require purification, auxiliary treatment and functionalization steps. In this regard, conducting polymers with tunable conductivity and non-transparency to microwaves can offer an attractive solution for efficient handling of EM pollution^{1,3,6,8-12}. These macromolecules have attained a special status in the area of material science due to novel structural, optoelectronic and electromagnetic properties¹³⁻¹⁶ and broad spectrum of application covering energy storage, gas/bio-sensors, corrosion inhibition, EMI shielding, electrostatic dissipation (ESD), organic light emitting diodes, photovoltaics^{1,6,12,17-22} etc. Among other conducting polymers, polyaniline (PANI) has received enormous attention due to distinguished advantages like low monomer cost, facile synthesis, non-corrosiveness, good environmental/thermal stability and tunable electrical/electromagnetic attributes^{3,6,10,11,13,15,23}. Its electrical properties and polarization response can easily be tuned by adjusting the oxidation state and degree of doping of the backbone making it a promising material for future techno-commercial applications. Chemically, polyaniline is made up of benzenoid and quinoid units such that preferential

protonation of iminine nitrogen atoms convert insulating emeraldine base (EB, 50% oxidized and 50% reduced form) convert it into emeraldine salt (ES) via formation of charge carriers i.e. polarons/bipolarons which impart polarization and electrical conductivity^{24,25} to the PANI. Interestingly, high conductivity and dielectric constant of the materials contribute to high EMI shielding efficiency^{3,26}. Due to polaronic defects only doped conducting polymers like PANI exhibit good EMI absorbing properties as compared to metals because they do not only reflect but selectively absorb electromagnetic radiations also. Therefore, protonic acid doping plays a critical role in determining the microwave shielding response of polyaniline and systematic studies in this direction are necessary. However, few brief studies^{23,26} on the doping process of PANI, is available. In the present study, we have prepared doped PANI samples by protonation of EB with different concentration of *para*-toluene sulfonic acid (PTSA) dopant. These samples have been characterized for spectral, thermal, magnetic, electrical and electromagnetic attributes to enlighten the effect of dopant concentration on electrical conductivity as well as dielectric attributes which are of paramount importance for determining the related EMI shielding response.

2 Experimental Details

Aniline (Loba Chemie, India) was freshly double distilled before use. Analytical grade hydrochloric acid (35.5% HCl, Merck), ammonia (25% aqueous solution), *para* toluene sulfonic acid (PTSA, Merck) and ammonium peroxydisulfate (APS, Merck) were used without on as received basis. Aqueous solutions were prepared from the Millipore water of resistivity value 18 M Ω -cm.

The polyaniline was prepared by chemical oxidative polymerization. In a typical synthesis, 0.1 mol of aniline and 1.0 mol of HCl were mixed in 1.0 L of distilled water. The polymerization was initiated by the drop wise addition of pre-cooled aqueous solution of ammonium persulphate (APS) [0.1 mol, (NH₄)₂S₂O₈ in 100 ml H₂O]. The polymerization was carried out at a temperature of -2.0°C under continuous stirring so as to maintain reaction homogeneity throughout the bulk and to control the reaction exothermicity. After completion of polymerization, the polymer has been formed directly in the doped state as a dark green precipitate dispersed in the reaction mixture. The polymer was isolated from the reaction mixture as a dense cake by

filtration and washed repeatedly with distilled water till the filtrate became colorless and neutral. The repeated washings help in removing oxidant and oligomeric impurities as well as any free dopant (HCl) moiety from the polymer. The washed polymer cake was then dried under vacuum at 50°C and crushed to obtain the powder of the doped polymer designated as PANI-HCl. The above-synthesized powder (PANI-HCl) was then treated with 0.1 M aqueous ammonia and stirred for 2 h to remove the dopant by neutralization to obtain the undoped i.e. emeraldine base (EB) form of the polymer. The EB powder was then obtained by the processes of filtration, rinsing, drying and crushing successively. The redoping was performed by taking 1.0 g of the EB and treating it with 0.0001, 0.001, 0.01, 0.1, 0.5 M and 1.0 M aqueous solution of PTSA for 2 h leading to formation of PTSA doped PANI samples designated as ES1, ES2, ES3, ES4, ES5 and ES6, respectively.

IR transmission spectra of samples in KBr pellet form were recorded using GX-2000 Perkin Elmer FTIR spectrophotometer in the wave number range 4000-400 cm⁻¹ and at a resolution of 4 cm⁻¹ averaged over 32 number of scans. The UV-vis.-spectra recorded on a Shimadzu 1601 UV-Visible spectrometer in the wavelength range 200-1100 nm and using quartz cuvettes of 1.0 cm path length. Morphologies were recorded from scanning electron microscope (SEM, Leo-440, UK). The thermal stability measurements in the temperature range 25-700°C were performed under inert atmosphere of flowing nitrogen gas (60 ml/min) and using TGA (Mettler Toledo TGA/SDTA 851^c, Switzerland) system at a constant heating rate of 10°C/min. The materials were heated. Rectangular pellets (13 mm × 7 mm × 2 mm) were prepared by hydraulic press (compression pressure of 5 ton) and used for electrical conductivity measurements at room temperature by four probe technique using programmable current source (Keithley 220) and a nanovoltmeter (Keithley 181). Shielding effectiveness (SE) and electromagnetic attributes (complex permittivity and permeability) were measured using a vector network analyzer (VNA, Model: E8263B, Agilent Technologies), by placing pressed pellets inside a sample holder connected between the flange of Ku-band (12.4-18.0 GHz) coaxial-to-waveguide adaptors. Electron paramagnetic resonance (EPR) spectra were recorded on Varian make X-band CW E-line Century E-112 EPR spectrometer at 300 K temperature. Equal weights of powdered samples

were filled in fine quartz capillary tubes of ~ 1 mm internal diameter. The sample tubes were placed in the centre of EPR rectangular cavity. The magnetic field was modulated at 100 kHz frequency at low modulation amplitude to avoid any distortion in EPR line shape. 10 mW microwave power was used to avoid any saturation effect. 1,1-diphenyl 2-picryl hydrazyl (DPPH) was used as a standard reference sample for g -value and the spin concentration determination.

3 Results and Discussion

The SEM image of ES6 (Fig. 1) powder displays highly agglomerated morphology made up of fibrous particle with 100-200 nm in diameter and 800-900 nm in length.

These particles are formed during low temperature *in-situ* polymerization of aniline and maintained their morphology even after redoping with PTSA, but agglomeration appeared due to strong intra and intermolecular ionic interactions between chains triggered by protogenerated charge carriers (i.e. polarons/bipolarons). Nevertheless, such quasi-one dimensional electrically conducting particles are already known to form mechanically strong, porous and sufficiently conducting films that can display improved cyclic performance as electrode materials of redox-supercapacitors/batteries or fast response for sensors/actuators²⁷⁻²⁹. It is worth to mention that fibrous and tubular nanostructured conjugated polymers with good electrical, electromagnetic or electrochemical properties are an important candidate for frontier applications like EMI shielding^{3,11} and needs further analysis of their electrical and electromagnetic properties.

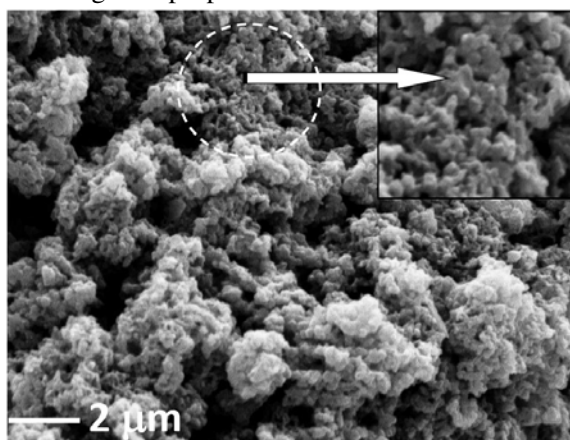


Fig. 1 — SEM image of ES6 (PANI-PTSA-1.0 M) showing fibrous morphology. Inset shows the magnified image of encircled region

FTIR of EB (Fig. 2a) shows characteristics bands at 1588 cm^{-1} and 1497 cm^{-1} due to C=C stretching of the quinoid diimine (N=Q=N) and benzenoid diamine (N-B-N) segments, respectively. In addition, C-N stretching absorption at 1377 cm^{-1} along with prominent bands at 1305 cm^{-1} (C=N stretching) and 1163 cm^{-1} (in-plane bending of the C-H bond of N=Q=N segments) were also observed.

The presence of out-of-plane C-H bending vibrations of *para* di-substituted benzene rings at 826 cm^{-1} confirms the formation of head-to-tail *para*-coupled polymer²⁵. The doping of emeraldine base units results in protonation of the imine nitrogen atoms leading to systematic shift in the position and relative intensity of its characteristic bands with change in dopant concentration. In particular, FTIR spectrum (Fig. 2b) of ES6 (PANI:1M PTSA) displays the stretching vibration of hydrogen bonded secondary amine group as a strong broad band at 3447 cm^{-1} whereas peaks at 1562 (green arrow) and 1478 cm^{-1} (magenta arrow) are attributed to substituted benzenoid (B) and quinoid (Q) rings, respectively.

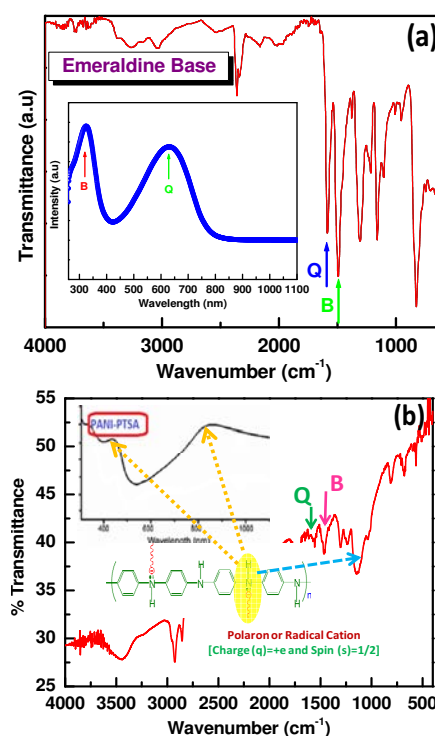


Fig. 2 — FTIR transmittance spectrum of (a) EB and (b) ES6 with highlighted quenoid (Q), benzenoid (B) and polaronic (blue arrow) stretching vibrations; Inset Fig. 2(a) shows the UV-visible absorption spectra of EB whereas inset Fig. 2(b) displays schematic of polaron on polyaniline unit and uv-visible absorption spectra of ES6 with marked (orange arrows) polaronic transitions

The protonation of EB by PTSA initially generates bipolarons (dications) which undergoing an internal redox reaction (induced spin unpairing where Q units are converted into B units) and transforms to paramagnetic polarons (Fig. 3). These further separate out due to their electrostatic repulsion leading to the formation of radical cations (or polarons), which is marked by the presence of a prominent signature at 1298 cm^{-1} . The strong and broad p-toulene sulfonate ion stretching vibration and C–H bending of Q ring (marked by blue arrow) is observed at 1120 cm^{-1} . The appearance of this peak confirms the high degree of electron delocalization in PANI polymeric chain²⁵ and can be attributed to presence of polarons (shown schematically in inset of Fig. 1b) on PANI backbone. The same has been complemented by UV-visible absorption spectra of ES6 which also show polaronic transitions (orange arrows) around 460 nm and 855 nm along with $\pi_B \rightarrow \pi_B^*$ (or band gap) transitions of doped PANI at 360 nm. Since the polarons are paramagnetic charge carriers, their concentration and mobility determine the polarization, magnetic properties, electrical conductivity, conduction mechanism as well as electromagnetic response. Therefore, rest of the paper deals with the qualitative and quantitative analysis of the polaron concentration

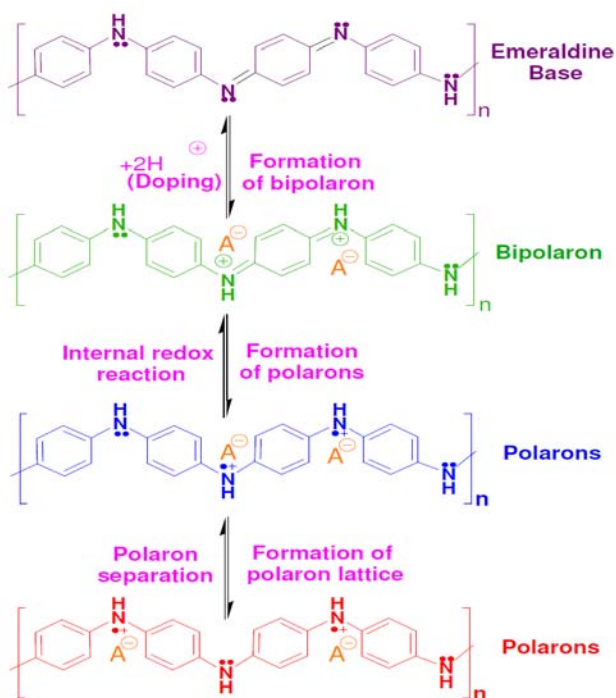


Fig. 3 — Schematic representation of doping process involving formation of bipolarons and polarons via non-redox doping involving protonic acids

and its properties e.g. conduction, polarization and attenuation of EM energy.

Figure 4 shows the thermogravimetric (TG) traces of three different doped samples. It has been observed that samples doped with different concentrations of PTSA display a small initial mass loss between $25\text{--}100^\circ\text{C}$ that can be attributed to the adsorbed moisture. As the doping level increases, this loss increases from $\sim 2\text{ wt}\%$ (ES3) to $\sim 5\text{ wt}\%$ (ES6). It is well known that EB display good thermal stability ($>440^\circ\text{C}$) after which it loses 30% mass²⁵ up to 700°C . However, the introduction of dopant and enhancement of doping level lead to systematic decrease in the thermal stability of the samples e.g. the initial decomposition temperature (IDT) of ES3 was 273°C which decreases to 240°C for ES6. This can be attributed to doping induced conversion of quinoid units to benzenoid segments and overlapping of dopant degradation step (stable up to 300°C) with decomposition temperature (that continued till 700°C) of polymeric backbone. Therefore, among doped polymers, mass loss between $120\text{--}300^\circ\text{C}$ was used for qualitative (semi-quantitative) estimation of doping level and results (Table 1) revealed that up to ES3 doping level was low (\sim one polarons per 60 rings) but increases rapidly afterwards and becomes \sim one polarons per 4 rings for ES6. As the polarons are known to have pronounced polarization effects; therefore, ES6 is expected to display best electromagnetic response. It is further clear from the above studies that though doping enhances conductivity, it does so at the expense of thermal stability. Nevertheless, all doped samples have thermal stability in excess of 230°C i.e. greater than melt processing temperatures of conventional thermoplastics like low density polyethylene ($150\text{--}160^\circ\text{C}$) or polypropylene ($210\text{--}220^\circ\text{C}$), which

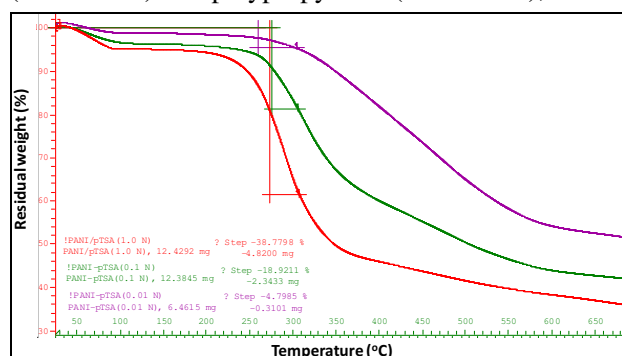


Fig. 4 — TGA curves of PTSA doped PANI samples displaying moisture loss and degradation steps along with char residues at 700°C

Table 1 — Effect of PTSA concentration on the thermal, electrical and electromagnetic attributes of samples

S. No.	Dopant Conc. (M)	Sample Designation	TGA (% mass loss between 120 & 300°C)	DC Electrical Conductivity (S/cm)	Real and Imaginary permittivity (ϵ' , ϵ'')	Shielding Effectiveness (dB)
1.	0	EB	~0	1.2×10^{-9}	5.5, 0.6	-3.8
2.	0.0001	ES1	~0.2	0.0025	8.4, 4.5	-5.2
3.	0.001	ES2	~0.9	0.01	11.1, 9.7	-8.7
4.	0.01	ES3	~3	0.11	13.2, 13.1	-12.1
5.	0.1	ES4	~14	1.21	15.8, 17.8	-17.2
6.	0.5	ES5	~27	1.82	17.5, 19.8	-19.5
7.	1.0	ES6	~33	5.31	22.3, 24.6	-23.9

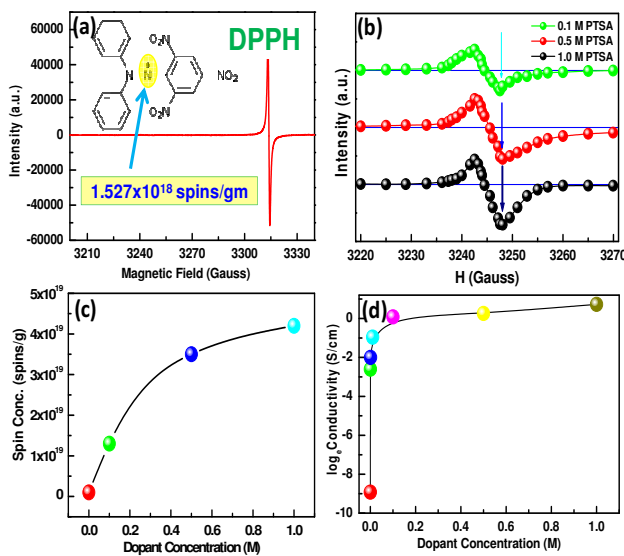


Fig. 5 — EPR spectra of (a) standard DPPH and (b) different PTSA doped samples, Variation of (c) spin concentration versus dopant concentration and (d) electrical conductivity of PANI samples as a function of versus dopant concentration plots

suggest that these materials could be processed via melt blending route.

It is worth noting that when two adjacent polarons separate out, doped polyaniline becomes paramagnetic. EPR spectrum of DPPH standard is shown in Fig. 5(a) and displays an intense narrow signal. In contrast, spectra (Fig. 5b) of higher doping level samples (i.e. ES4, ES5 and ES6) consist of narrow single Lorentzian shaped resonance line signal with the Dysonian contribution indicating intrinsic conductivity of metal-like domains³⁰⁻³⁵.

EPR parameters derived from these spectra are listed in Table 2. The Dysonian asymmetry in line shape is, generally, observed in metallic samples and appears when the skin depth becomes smaller than the sample thickness³¹. The asymmetry increases [arrows in Fig. 5(b)] with dopant concentration indicating increase in metallic character and presence of mobile

Table 2 — EPR parameters EB and PTSA doped samples

S. No.	Sample	g -value	Spin-spin relaxation time constant T_2 (sec)	Line-width (Gauss)	Spin concentration (Spins/g)
1.	EB	2.0039	3.2749×10^{-11}	10.0	2.6×10^{18}
2.	ES4	2.0040	3.8984×10^{-11}	8.4	1.3×10^{19}
3.	ES5	2.0040	4.3088×10^{-11}	7.6	3.5×10^{19}
4.	ES6	2.0039	5.9542×10^{-11}	5.5	4.2×10^{19}

spin carrying species in the system. The g -values remained in the range 2.0039-2.0040 i.e. close to free electron g -value (2.0023), which suggests that the resonance arises from the electrons delocalized in the π -bonded system of these conjugated polymeric systems consisting of p_z orbitals of carbon and nitrogen atoms in the main chain of polyaniline. The decrease in peak-to-peak linewidth with increase in doping concentration confirms the existence of mobile polarons. Hence, the linewidth of EPR signal is a direct measure of the quality of metallic domains in conducting polymer, i.e. narrower the line, the more perfect and ordered are the doped regions. The spin concentration of the polaronic charge carriers has been determined by comparison method using DPPH as standard reference material which increases from 10^{18} to 10^{19} spins/g with increase in the doping level. This increase in charge carrier concentration results into enhanced electrical conductivity (Fig. 5d) of the doped samples. The increasing dopant concentration not only increases the density of proto-generated charge carriers (as evident from EPR spin concentration shown in inset of Fig. 5b) but also leads to increased mobility (EPR linewidth), resulting in enhancement of conductivity from $\sim 10^{-9}$ S/cm for EB to 0.0025 S/cm (about six orders increase) for the least doped sample (ES1). The conductivity further increases with dopant concentration and becomes

5.31 S/cm for ES6. Interestingly, the spin-spin relaxation process is characterized by a time constant (i.e. T_2), which is a function of static magnetic field. It depends on the rate of absorption and dissipation of microwave energy and can be expressed as⁶ :

$$\frac{1}{T_2} (\text{sec}^{-1}) = \frac{2\pi g \beta \sqrt{3} \Delta H_{pp}}{h} \quad \dots(1)$$

where β and h are Bohr magneton ($= 9.274 \times 10^{-21}$ erg G^{-1}) and Planck's constant (6.626×10^{-29} erg s), respectively. The spin-spin relaxation time constant increases (Table 2) with increase in PTSA concentration and the spin-spin relaxation time of ES6 is almost double as compared to EB. This means that ES4 (with highest spin concentration, narrowest linewidth and highest relaxation times) possess highest microwave absorption property and shallowest skin depth which ultimately get reflected in best shielding performance.

It is worth mentioning that the conductivity of higher doping level samples (ES4, ES5 and ES6) is suitable for displaying efficient EMI shielding response¹. In actual practice, EMI shielding depends on the shield material's intrinsic properties (electrical conductivity, dielectric constant/real permittivity, dielectric dissipation/imaginary permittivity, real/imaginary permeability etc.) as well as extrinsic parameters like geometry or thickness³. The radiation blocking efficiency of shield is measured in terms of quantity called shielding effectiveness (SE_T) and can be expressed^{1-3,6,16,23,26,36} as :

$$\begin{aligned} SE_T (dB) &= (SE_R + SE_A + SE_M) = 10 \log_{10} \left(\frac{P_T}{P_I} \right) \\ &= 20 \log_{10} \left(\frac{E_T}{E_I} \right) = 20 \log_{10} \left(\frac{H_T}{H_I} \right) \end{aligned} \quad \dots(2)$$

where P_I (E_I or H_I) and P_T (E_T or H_T) are the power (electric or magnetic field intensity) of incident and transmitted EM waves, respectively. The terms SE_R , SE_A and SE_M represent shielding due to reflection, absorption and multiple reflections (re-reflections), respectively and can be further written as:

$$SE_R (dB) = -20 \log_{10} \left(\frac{|1+n|^2}{4|n|} \right) \quad \dots(3)$$

$$SE_A (dB) = -20 \alpha t \log_{10} e = -8.68 \alpha t \quad \dots(4)$$

$$SE_M = -20 \log_{10} \left[1 - \left(\frac{|1-n|^2}{|1+n|^2} \right) \cdot \exp(-2\gamma t) \right] \quad \dots(5)$$

$$\alpha = \frac{1}{\delta} = \frac{2\pi}{\lambda_o} \sqrt{\frac{\epsilon_r (\sqrt{1 + \tan \delta \mp 1})}{2}} \quad \dots(6)$$

$$n = \sqrt{\frac{\epsilon_r (\sqrt{1 + \tan \delta \pm 1})}{2}} + i \sqrt{\frac{\epsilon_r (\sqrt{1 + \tan \delta \mp 1})}{2}} \quad \dots(7)$$

$$\gamma = \frac{2\pi}{\lambda_o} \left[\sqrt{\frac{\epsilon_r (\sqrt{1 + \tan \delta \mp 1})}{2}} + i \sqrt{\frac{\epsilon_r (\sqrt{1 + \tan \delta \pm 1})}{2}} \right] \quad \dots(8)$$

Here, n is the complex refractive index, γ is propagation constant, α is attenuation constant and t is thickness of the shielding material. The parameter skin depth ($\delta = 1/\alpha$) is defined as the depth of penetration at which the incident EM radiation is reduced to 33% of its original strength. If $\epsilon'(\mu')$ and $\epsilon''(\mu'')$ represent real and imaginary parts of complex permittivity (permeability), respectively, the terms loss tangent and total conductivity (σ_T) can be written as $\tan \delta (\epsilon''/\epsilon')$ and $\sigma_{ac} = (\sigma_{ac} + \sigma_{dc}) \omega \epsilon_0 \epsilon'$. Therefore, we may write:

$$\tan \delta = \frac{\sigma_T}{\omega \epsilon_0 \epsilon'} \quad \dots(9)$$

where σ_{ac} and σ_{dc} are frequency ($f = \omega/2\pi$) dependent (ac) and independent (dc) components of σ_T Eqs 6 and 9 reveal that for moderately conducting and non-magnetic materials ($\mu \sim 1$ & $\mu'' \sim 0$), i.e. both electrical conductivity as well as permittivity are important for enhancement of absorption loss and total shielding effectiveness.

Figure 6(a) shows the frequency dependence of SE_T values for EB and ES6 samples whereas inset of Fig. 6(a) display variation of real and imaginary permittivity of EB and ES6 with increasing frequency. It can be seen that pure EB with poor electrical conductivity ($\sim 10^{-9}$ S/cm) and permittivity ($\epsilon' \sim 5.5$ and $\epsilon'' \sim 0.6$) values (Table 1), gives very low attenuation i.e. only -3.8 dB. However, doping led to generation of polarons with associated electrical conduction and polarization effects resulting in systematic enhancement of SE_T value from -5.3 dB (for ES1) to -23.9 dB (for ES6 i.e. $>99\%$ attenuation

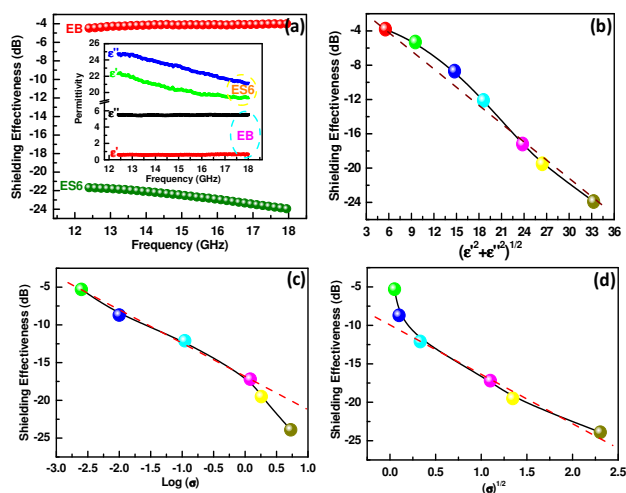


Fig. 6 — Frequency dependence of shielding effectiveness (SE_T) as well as for EB and ES6. Inset shows variation of real permittivity (ϵ') and imaginary permittivity (ϵ'') with frequency

with $\epsilon' \sim 22.3$ and $\epsilon'' \sim 24.6$). Additionally, the experimental SE_T values follow the patterns of permittivity (Fig. 6b) and conductivity [Fig. 6(c and d)]. In order to probe further, shielding response is studied under good conductor approximation when SE_T can be expressed^{16,23} as :

$$SE_T (\text{dB}) = -10 \log_{10} \left(\frac{\sigma_T}{16\omega\epsilon\mu_T} \right) - 8.68t \left(\frac{\sigma_T \omega \mu_T}{2} \right)^{1/2} \dots (10)$$

where first and second terms represent reflective and absorptive attenuation, respectively. Fig. 6 (c and d) shows the variation of SE_T (dB) with $\log(\sigma_T)$ and $(\sigma_T)^{1/2}$, respectively. The results revealed that logarithmic conductivity dependence shows linearity for low conductivity samples and deviates from linearity for highly doped samples. In contrast, opposite trend was observed for square root conductivity dependence of SET. These results revealed that at doping reflection plays the major role whereas at higher doping levels absorption attenuation becomes increasingly important. This can be again attributed to the enhancement of polaronic concentration leading to improvement of electrical conductivity as well as dielectric properties both of which are important to achieve high attenuation.

4 Conclusions

Doped PANI samples have been prepared by protonation of EB with different concentration of *p*-toluene sulfonic acid (PTSA) and systematically characterized so as to unfold the effect of dopant

concentration on electrical and dielectric properties and related EMI shielding response. The results revealed that both electrical conductivity as well as permittivity increase with dopant concentration due to increase in concentration polaronic defects which are known to display charge conduction ability and polarization effects. The undoped PANI (EB) gives very low attenuation of -3.8 dB which increases to -23.9 dB for 1.0 M PTSA doped sample. Further, the shielding dependence of permittivity and conductivity revealed that both polarization as well as conduction is important for achieving high attenuation. It was also observed that at low doping level reflection plays the major role whereas at higher doping level absorption contribution tends to dominate total attenuation.

Acknowledgement

The authors are grateful to Director, CSIR-NPL, New Delhi for according permission to publish the work. Encouragement and support for the work by Prof. Vikram Kumar, Ex Director, CSIR-NPL is also gratefully acknowledged.

References

- Saini P & Arora M, *New Polymers for Special Applications*, (ed.) Intech: Croatia, (2012) 71.
- Yang Y, Gupta M C, Dudley K L & Lawrence R W, *Nanolett*, 5 (2005) 2131.
- Saini P, Choudhary V, Singh B P, Mathur R B & Dhawan S K, *Mater Chem Phys*, 113 (2009) 919.
- Liu Q, Gu J, Zhang W, Miyamoto Y, Chen Z & Zhang D, *J Mater Chem*, 22 (2012) 21183.
- Li N, Huang Y, Du F, He X, Lin X, Gao H, Ma Y, Li F, Chen Y & Eklund P C, *Nano Lett*, 6 (2006) 1141.
- Saini P, Arora M, Gupta G, Gupta B K, Singh V N & Choudhary V, *Nanoscale*, 5 (2013) 4330.
- Wang H, Wang G, Li W, Wang Q, Wei W, Jiang Z & Zhang S, *J Mater Chem*, 22 (2012) 21232.
- Lakshmi K, John H, Mathew K T, Joseph R & George K E, *Acta Materialia*, 57 (2009) 371.
- Saini P, Choudhary V, Singh B P, Mathur R B & Dhawan S K, *Synth Met*, 161 (2011) 1522.
- Freund M S & Deore B, *Self-Doped Conducting Polymers*, John Wiley & Sons Ltd. Chichester, Chapter 2, p 123.
- Trivedi D C, *Handbook of Organic Conductive Molecules and Polymers*, Wiley, New York, 2 (1997) 505.
- Saini P & Choudhary V, *J Mater Sci*, 48 (2013) 797.
- Skotheim T A, *Handbook of Conducting Polymers*, 2nd Edition, CRC, (1986).
- Saini P, Choudhary V, Vijayan N & Kotnala R K, *J Phys Chem C*, 116 (2012) 13403.
- Cao Y, Smith P & Heeger A J, *Synth Met*, 48 (1992) 91.
- Colaneri N F & Shacklette L W, *IEEE Trans Instrum Meas*, 41 (1992) 291.
- Jung J W, Lee J U & Jo W H, *J Phys Chem C*, 114 (2010) 633.

- 18 Wycisk R, Pozniak R & Pasternak A, *J Electrostat*, 56 (2002) 55.
- 19 Saini P & Choudhary V, *J Nanoparticle Res*, 15 (2013) 1415.
- 20 Saini P & Choudhary V, *Indian J Pure Appl Phys*, 51 (2013) 112.
- 21 Zhang H, Cao G, Wang Z, Yang Y, Shi Z & Gu Z, *Electrochem Solid-State Lett*, 11 (2008) 223.
- 22 Bai H & Shi G, *Sensors*, 7 (2007) 267.
- 23 Saini P & Arora M, *J Mater Chem A1*, (2013) 8926.
- 24 Mattosso L H C, Faria R M, Bulhoes L O S, MacDiarmid A G & Epstein A J, *J Polym Sci A Polym Chem*, 32 (1994) 2147.
- 25 Saini P, Jalan R & Dhawan S K, *J Appl Polym Sci*, 108 (2008) 1437.
- 26 Joo J, Song H G, Jang K S & Oh E J, *Synth Met* 102 (1999) 1349.
- 27 Gupta V & Miura N, *Mater Lett*, 60 (2006) 1466.
- 28 Wang Y G, Li H Q & Xia Y Y, *Adv Mater*, 18 (2006) 2619.
- 29 Kim S H, Oh K W & Choi J H, *J Appl Polym Sci*, 116 (2010) 2601.
- 30 Wertz J E & Boulton J R, *Electron Spin Resonance*, MC Graw Hill Book Company, New York, (1972).
- 31 Dyson F J, *Phys Rev*, 98 (1955) 349.
- 32 Krinichnyi V I, Roth, H-K, Schrodner M & Wessling B, *Polymer*, 47 (2006) 7460.
- 33 Alger R S, *Electron paramagnetic resonance, Technique & Applications* (New York: Interscience Publishers), (1968) 494.
- 34 Krinichnyi V I, Tokarev S V, Roth H K, Schrodner M & Wessling B, *Synth Metals*, 156 (2006) 1368.
- 35 Kahol P K, Dyakonov A J & McCormick B J, *Synthetic Metals*, 84 (1997) 691.
- 36 Saini P, Choudhary V, Sood K N & Dhawan S K, *J Appl Polym Sci*, 113 (2009) 3146.